2D Materials

PAPER

# Equi-biaxial compressive strain in graphene: Grüneisen parameter and buckling ridges

RECEIVED
25 August 2018

REVISED
1 November 2018

ACCEPTED FOR PUBLICATION
19 November 2018

PUBLISHED
10 December 2018

Tao Jiang[1,5], Zuyuan Wang[2,4], Xiulin Ruan[2] and Yong Zhu[3,5]

[1] School of Materials Science and Engineering, University of Jinan, Jinan, Shandong 250022, People's Republic of China
[2] School of Mechanical Engineering and the Birck Nanotechnology Center, Purdue University, West Lafayette, IN 47907, United States of America
[3] Department of Mechanical and Aerospace Engineering, North Carolina State University, Raleigh, NC 27695, United States of America
[4] Present Address: Max Planck Institute for Polymer Research, Ackermannweg 10, Mainz 55128, Germany
[5] Author to whom any correspondence should be addressed

**E-mail:** mse_jiangt@ujn.edu.cn (T Jiang) and yzhu7@ncsu.edu (Y Zhu)

Supplementary material for this article is available online

**Keywords:** biaxial strain, buckling ridges, graphene, Grüneisen parameter, thermal cycling, molecular dynamics simulation

## Abstract

Strain and defects in graphene have critical impact on morphology and properties of graphene. Here we report equi-biaxial compressive strain in monolayer graphene on $SiO_2$ and $Si_3N_4$ substrates induced by thermal cycling in vacuum. The equi-biaxial strain is attributed to the mismatch in coefficient of thermal expansion between graphene and the substrate and sliding of graphene on the substrate. The sliding occurs during heating at the temperatures of 390 and 360 K for graphene on $SiO_2$ and $Si_3N_4$ substrates, respectively. The biaxial Grüneisen parameter is determined to be 1.95 and 3.15 for $G$ and $2D$ Raman bands of graphene, respectively. As the heating temperature exceeds a threshold temperature (1040 K for graphene/$SiO_2$ and 640 K for graphene/$Si_3N_4$), buckling ridges are observed in graphene after the thermal cycle, from which the biaxial buckling strain of graphene on $SiO_2$ and $Si_3N_4$ substrates are obtained as 0.21% and 0.22%, respectively. Importantly, the induced buckling ridges in graphene exhibit a pattern representing the symmetry of graphene crystal structure, which indicates that graphene relieves the compressive stress mainly along its lattice symmetry directions. These thermally induced graphene ridges are also found reminiscent of those in the synthesized graphene, suggesting the same origin of formation of the buckling ridges under biaxial compression.

## Introduction

Graphene has shown great promise for a broad range of applications including flexible and stretchable electronics [1, 2], composite materials [3, 4], and nanoelectromechanical systems [5, 6]. In general, it has been known that strain can dramatically influence electronic, mechanical, optical and other properties of monolayer graphene [7–10]. For example, strain in graphene can lead to bandgap opening [11, 12], zero-field quantum Hall effect [13, 14], topological phases [15, 16], pseudo-magnetic field [17, 18], etc. In particular, biaxial stain in graphene can enhance the electron–phonon coupling [19], leading to superconductivity [19, 20]. For most applications, graphene is deposited on substrates (or in matrices). Because graphene is ultra-thin with an extremely high surface-to-volume ratio, like all two-dimensional materials, its morphology and properties are susceptible to the substrates. For example, when graphene-based devices undergo temperature cycles, strain (or stress) in graphene can arise as a result of the difference in coefficient of thermal expansion (CTE) between graphene and substrates. It is of important relevance to understand how such a strain can modulate the morphology and properties of graphene, thus affect performances and reliability of the graphene-based devices.

In spite of recent advances, two important issues related to strain in graphene remain unclear—Grüneisen parameter and compressive strain induced buckling ridges. Previously reported values of Grüneisen parameter of graphene—a fundamental physical parameter—exhibited large discrepancy [21, 22]

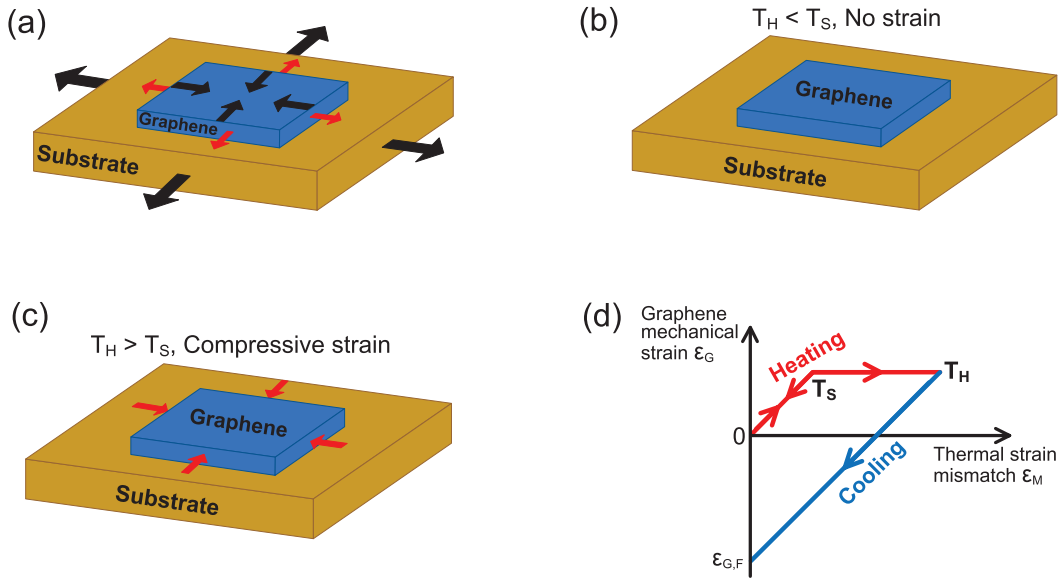


**Figure 1.** Schematic of the induced strain in graphene by the heating-cooling cycle. (a) Thermal expansion of substrate and contraction of graphene during heating. The black arrows designate the thermal strains in graphene and substrate. The red arrows designate the mechanical strain in graphene exerted by the substrate due to their CTE mismatch. (b) No strain is induced in graphene by the heating-cooling cycle for $T_H < T_S$. (c) For $T_H > T_S$, the cycling induces compressive strain (red arrow) in graphene. (d) Schematic of how the mechanical strain in graphene $\varepsilon_G$ changes with the mismatch of thermal strain $\varepsilon_M$ during a heating-cooling cycle. Note that $\varepsilon_{G,F}$—the final strain in graphene after the cycle—is compressive (negative).

and there is no commonly accepted value to date [23]. Moreover, most studies were carried out under uniaxial strain, not biaxial strain, which is pertinent to most applications where graphene is placed on a substrate. Most of the reported studies on the compression behavior of graphene were limited to measuring the Raman spectrum of graphene under uniaxial strain (e.g. loaded by a flexible substrate) [24–27]. It has been reported that buckling ridges can be generated when the compressive strain exceeds a certain threshold [26]. Nevertheless, few studies have investigated the morphology of the buckling ridges, especially the ridge network formed under biaxial compression [28]. Interestingly, similar ridge networks are commonly seen in graphene synthesized by chemical vapor deposition (CVD) [29, 30] or epitaxial growth method [31].

Here we report a simple and robust method to introduce well-controlled equi-biaxial compressive strain in monolayer graphene on a substrate via thermal cycling in vacuum. A perfectly equi-biaxial strain is introduced in graphene due to the mismatch in CTE between graphene and the substrate and the sliding of graphene on the substrate. When the heating temperature is relatively low, no compressive strain is applied in graphene after the temperature cycle (i.e. back to room temperature). When the heating temperature exceeds a threshold temperature, beyond which graphene slides on the substrate, compressive strain arises. As the heating temperature further increases above a second threshold temperature, buckling ridge defects are generated in graphene at room temperature. Raman spectroscopy was employed to measure the biaxial strain in graphene, from which the biaxial Grüneisen parameter was reliably measured. In general, the Raman shift of graphene under strain depends on both the hydrostatic and shear components of the applied strain through the Grüneisen parameter and the shear deformation potential, respectively. Therefore, the perfectly equi-biaxial strain is very favorable in measurement of Grüneisen parameter due to its capability to avoid the shear effect. Importantly, the buckling ridges in graphene were found to occur in a pattern following the symmetry of graphene crystal structure, which agreed well with our molecular dynamics (MD) simulations. Furthermore, these thermally-induced buckling ridges were found reminiscent of those in graphene synthesized by the CVD and SiC sublimation methods, suggesting the same origin of formation of the buckling ridges.

## Results and discussion

### Temperature-cycling-induced biaxial strain in graphene

Monolayer graphene flakes were prepared by mechanical exfoliation [26, 32] on the Si-based substrate ($SiO_2$ or $Si_3N_4$) with dimensions of the flakes at tens of micrometers (e.g. $20 \times 30\ \mu m^2$). The samples were then subjected to a heating-cooling cycle (i.e. from room temperature to a heating temperature $T_H$ then back to room temperature). The strain in a graphene flake due to the CTE mismatch between graphene and substrate is depicted in figure 1(a) schematically. Because the CTE of substrate is positive while that of graphene is negative in the temperature range under study, it can be seen that the substrate

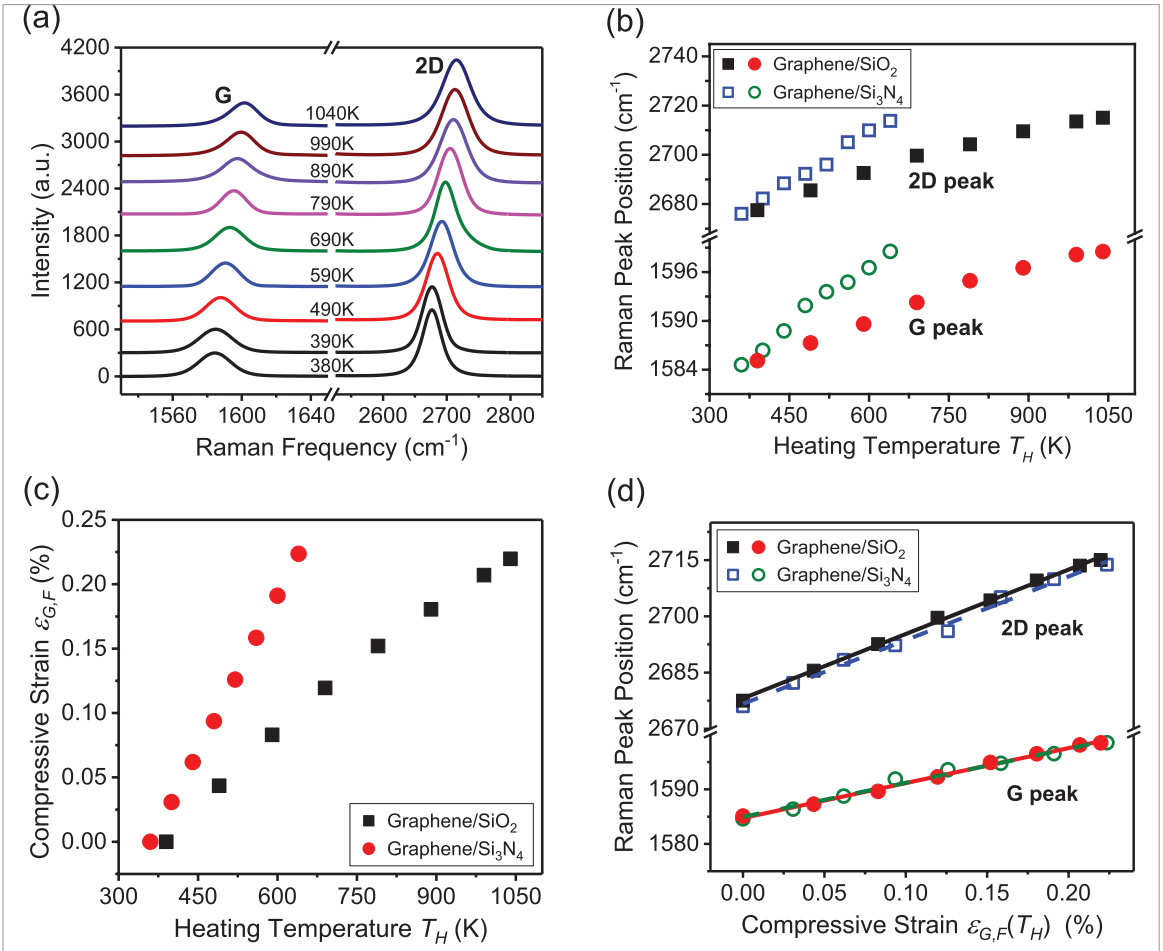


**Figure 2.** (a) Raman spectra of graphene on $SiO_2$ after the heating-cooling cycle at various heating temperature $T_H$. Both *G* and *2D* peaks blue shift as $T_H > 390$ K. (b) Raman *G* and *2D* peak positions change with heating temperature $T_H$ for graphene/$SiO_2$ and graphene/$Si_3N_4$, respectively. (c) The final compressive strain in graphene after the cycle $\varepsilon_{G,F}$ for each heating temperature $T_H$. (d) The measured Raman *G* and *2D* peak positions versus the final compressive strain in graphene $\varepsilon_{G,F}$ ($T_H$). The solid symbols represent graphene/$SiO_2$ samples (fitting in solid lines); the open symbols represent graphene/$Si_3N_4$ samples (fitting in dash lines). All the four fitting curves fall into linear relationships.

expands whereas the graphene flake contracts during heating (see black arrows in figure 1(a)). Hence an additional mechanical strain (tensile in this case) is exerted on the graphene flake by the substrate through the van der Waals (vdW) interaction between them (see red arrows in figure 1(a)). During the cooling process back to room temperature, the tensile strain in the graphene flake decreases.

After the heating-cooling cycle, it was found that if the heating temperature $T_H$ was relatively low, no strain in the graphene flake was observed according to the Raman spectrum. However, if the heating temperature $T_H$ exceeded a threshold temperature $T_S$, a net compressive strain was observed in the graphene flake. The cycling-induced net strains in the graphene flake for the two cases with $T_H < T_S$ and $T_H > T_S$ are shown in figures 1(b) and (c), respectively.

The above observations can be accounted for by whether onset of graphene sliding occurs during the heating-cooling cycle. It is known that graphene adheres to $SiO_2$ and $Si_3N_4$ substrates via vdW interaction [33–35]. During heating, a tensile strain is loaded in the graphene flake by the substrate, which increases with the heating temperature. As $T_H$ is lower than $T_S$, the vdW interaction is able to hold the graphene flake in place (i.e. no sliding). Note that $T_S$ is called the sliding temperature for the rest of the paper. During cooling to room temperature, the tensile strain in the graphene flake decreases to zero as the thermal strains in both graphene and substrate decrease to zero. As $T_H$ exceeds $T_S$, the vdW interaction is unable to hold the graphene flake any longer and hence the graphene flake starts to slide relative to the substrate. During cooling to room temperature, the tensile strain in the graphene flake decreases all the way and becomes compressive strain eventually. Sliding of graphene on various substrates such as $SiO_2$ [36, 37] and polyethylene terephthalate (PET) [26] under strain has been reported, by either heating the graphene/substrate [38] or stretching the substrate [39, 40]. Our experiment shows graphene will slide on $SiO_2$ or $Si_3N_4$ substrate under an equi-biaxial strain, as heating temperature exceeds the threshold temperature $T_S$.

Figure 1(d) schematically shows how the mechanical strain in the graphene flake $\varepsilon_G$ varies with the mismatch thermal strain $\varepsilon_M$—the strain produced solely by the CTE difference between graphene and substrate. Note that here $\varepsilon_G$ is at the center of the graphene

flake. One can see that for $T_H < T_S$ (no sliding), during heating $\varepsilon_G = \varepsilon_M$, indicating the tensile strain induced by the CTE mismatch, $\varepsilon_M$, is completely transferred to the graphene flake from the substrate; during cooling, $\varepsilon_G$ decreases to zero following the same path as that during heating. For $T_H > T_S$ (after sliding), the graphene strain $\varepsilon_G$ remains constant during heating; during cooling, $\varepsilon_G$ decreases at the same slope as $\varepsilon_M$, and when $\varepsilon_M$ reaches zero (back to room temperature), $\varepsilon_G$ becomes negative (compressive strain). According to the linear relationship in figure 1(d), the final strain in graphene after the cycle, $\varepsilon_{G,F}$, would be $\varepsilon_{G,F} = \varepsilon_M(T_S) - \varepsilon_M(T_H)$. Strictly speaking, the strain evolution in the graphene flake during the heating-cooling cycle follows a nonlinear relationship [26], which would require knowledge of the graphene-substrate interface mechanical property. The linear relationship is, however, a reasonable approximation.

It is known that the positions of Raman $G$ and $2D$ peaks of monolayer graphene blue (red) shift if graphene is under the compressive (tensile) strain [22,41]. To date Raman spectroscopy has become a major method to probe and measure the strain in graphene [42, 43]. In order to characterize quantitatively the strain of graphene in our experiment, Raman spectroscopy was performed at the center of each graphene flake for graphene/$SiO_2$ and graphene/$Si_3N_4$. It should be emphasized that the Raman measurement was at room temperature, after each heating-cooling cycle. The measured Raman $G$ and $2D$ spectra of graphene on $SiO_2$ substrate corresponding to various heating temperature $T_H$ are depicted in figure 2(a). For graphene/$SiO_2$, the $G$ and $2D$ spectra at $T_H = 380$ K are the same as those at $T_H = 390$ K, while blue shifts of the two spectra commence at $T_H > 390$ K, indicating the sliding temperature $T_S^{SiO_2} = 390$ K for graphene/$SiO_2$. The sliding temperature for graphene/$Si_3N_4$, $T_S^{Si_3N_4}$, was measured to be 360 K. The $G$ and $2D$ peak positions (obtained from the Lorentzian fitting) as functions of the heating temperature $T_H$ for graphene/$SiO_2$ and graphene/$Si_3N_4$ are plotted in figure 2(b), respectively. Interestingly, the positions of the $G$ and $2D$ peaks show linear relationships with the final compressive strain $\varepsilon_{G,F}$ in the graphene flake after each temperature cycle for both graphene/$SiO_2$ and graphene/$Si_3N_4$, as shown in figure 2(d). Again $\varepsilon_{G,F} = \varepsilon_M(T_S) - \varepsilon_M(T_H)$. The linear relationships here indicate that the linear approximation as shown in figure 1(d) is appropriate. It's worth noting that the Raman $G$ peak in figure 2(a) does not split as the applied strain increases (the heating temperature gets higher). This is because the applied strain is equi-biaxial. Splitting of the $G$ peak is caused by breaking of graphene symmetry, which lifts the double degeneracy of the $G$ band [44, 45]. As a result, the splitting happens only under uniaxial strain where a shear component exists, but not under the equi-biaxial strain.

**Biaxial Grüneisen parameter of graphene**

Because the compressive strain $\varepsilon_{G,F}$ induced in graphene by the heating-cooling cycle is originated by CTE mismatch between graphene and substrate, $\varepsilon_{G,F}$ can be calculated as:

$$\begin{aligned}\varepsilon_{G,F} &= \varepsilon_M(T_S) - \varepsilon_M(T_H)\\ &= \int_{T_R}^{T_S}\left(\alpha_{sub}(T) - \alpha_{gra}(T)\right)dT - \int_{T_R}^{T_H}\left(\alpha_{sub}(T) - \alpha_{gra}(T)\right)dT\\ &= \int_{T_H}^{T_S}\left(\alpha_{sub}(T) - \alpha_{gra}(T)\right)dT\end{aligned} \quad (1)$$

where $T_R = 295$ K is room temperature, $T_S$ is the sliding temperature, $T_H$ is the heating temperature ($T_H > T_S$), and $\alpha_{gra}(T)$ and $\alpha_{sub}(T)$ are CTEs as functions of temperature for graphene and substrate ($SiO_2$ or $Si_3N_4$) respectively [46–48]. It is worth noting that because the calculated strain in graphene $\varepsilon_{G,F}$ is produced by the mismatch of CTE between graphene and substrate through the graphene-substrate interaction (i.e. interfacial shear stress transfer between graphene and substrate [26,27]), here it needs to use the CTE of free-standing graphene [36, 49], not the CTE of graphene prepared on substrate [50, 51], in which the effect of graphene-substrate interaction has been included. By measuring the sliding temperature $T_S$ for graphene/$SiO_2$ and graphene/$Si_3N_4$, the final compressive strain in graphene after the cycle $\varepsilon_{G,F}$ for each heating temperature can be calculated using equation (1). The obtained $\varepsilon_{G,F}$ as a function of heating temperature $T_H$ for graphene/$SiO_2$ and graphene/$Si_3N_4$ are plotted in figure 2(c), in which the compressive strain increase with the increase of heating temperature for both graphene/$SiO_2$ and graphene/$Si_3N_4$, as expected. Of course equation (1) applies when $T_H$ is higher than $T_S$—when $T_H$ is lower than $T_S$, the strain in the graphene after cooling is zero. As shown by the CTEs of graphene [46], $SiO_2$ [47] and $Si_3N_4$ [48] (see figure S2(a) in supplementary material (stacks.iop.org/TDM/6/015026/mmedia)), $\alpha_{gra}(T) < 0$ but $\alpha_{SiO_2}(T) > 0$ and $\alpha_{Si_3N_4}(T) > 0$ in the range of working temperature, hence $\varepsilon_{G,F} < 0$.

The linear relationship shown in figure 2(d) agrees well with reports from others [41, 42]. The linear fitting in figure 2(d) yields, for the equi-biaxial strain, the peak position shift rate $\lambda$ to be $\lambda_G^{SiO_2} = 64.1$ cm$^{-1}$/%, $\lambda_G^{Si_3N_4} = 62.5$ cm$^{-1}$/%, $\lambda_{2D}^{SiO_2} = 171.8$ cm$^{-1}$/%, and $\lambda_{2D}^{Si_3N_4} = 169.9$ cm$^{-1}$/%, where $\lambda_G^{SiO_2}$, $\lambda_G^{Si_3N_4}$, $\lambda_{2D}^{SiO_2}$, and $\lambda_{2D}^{Si_3N_4}$ represent shift rates of $G$ peak for $SiO_2$, $G$ peak for $Si_3N_4$, $2D$ peak for $SiO_2$, and $2D$ peak for $Si_3N_4$ substrate, respectively. It can be seen that the measured values of $G$ and $2D$ peak shift rates are very close for graphene/$SiO_2$ and graphene/$Si_3N_4$ samples (variation <2.5%), indicating that the shift rates are independent of the substrate.

Correlating the measured Raman peak shift rate and the calculated compressive strain in graphene $\varepsilon_{G,F}$ allows us to obtain biaxial Grüneisen parameter for both Raman $G$ and $2D$ spectra of monolayer graphene. Grüneisen parameter $\gamma$, a measure of crystal lattice anharmonicity, can be expressed as follows [21, 22]:

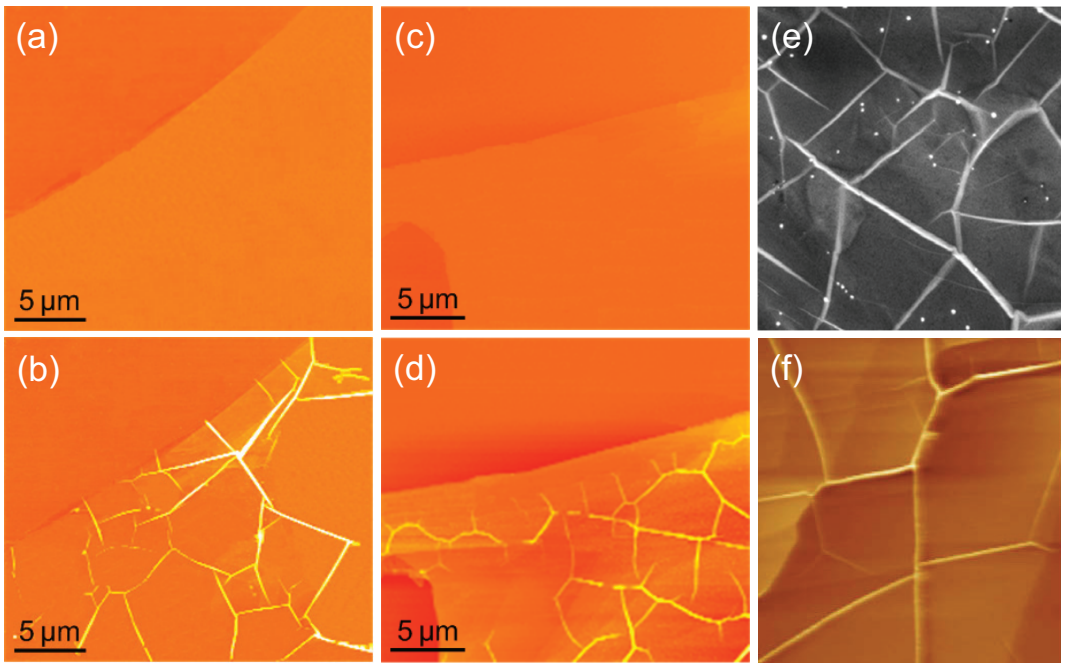


**Figure 3.** AFM images of monolayer graphene on $SiO_2$ (a) before and (b) after the heating-cooling cycle with $T_H = 1050$ K. AFM images of graphene on $Si_3N_4$ (c) before and (d) after heating-cooling cycle with $T_H = 650$ K. (e) and (f) Depict ridges on graphene synthesized on Ni by CVD [52] and synthesized on SiC by SiC sublimation [53], respectively.

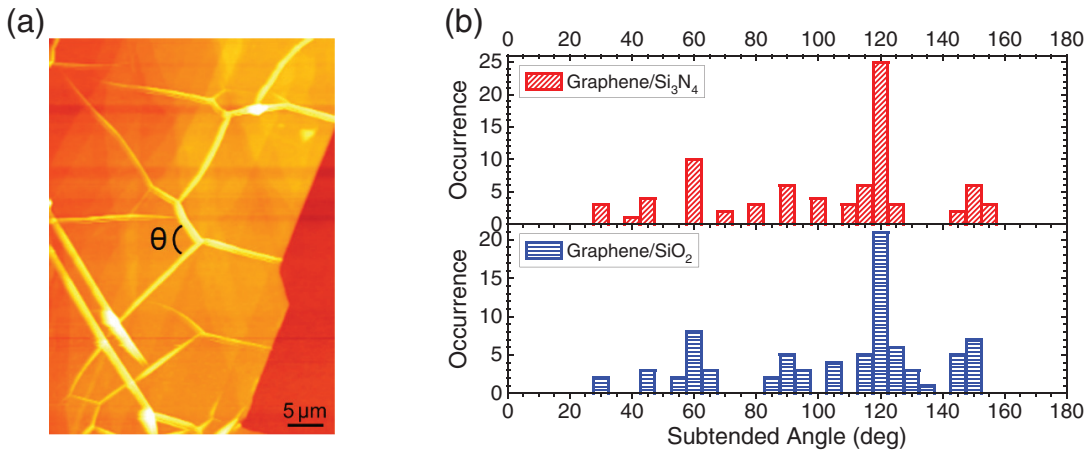


**Figure 4.** (a) AFM image of the buckling ridges generated on graphene/$SiO_2$ by the heating-cooling cycle. Angle $\theta$ designates the angle subtended between two ridges. (b) Histogram of the subtended angles between ridges in graphene/$SiO_2$ and graphene/$Si_3N_4$ respectively. In both cases, the subtended angle of 120° is most probable.

$$\gamma = \Delta\omega/2\varepsilon\omega_0 = \lambda/2\omega_0 \quad (2)$$

where $\Delta\omega$ is the Raman frequency shift, $\varepsilon$ is the strain, $\omega_0$ is the unstrained Raman frequency, and $\lambda = \Delta\omega/\varepsilon$ is the shift rate. As a fundamental physical quantity, Grüneisen parameter directly relates the phonon vibration of a crystal to its macroscopic thermal properties such as CTE and determines the thermodynamic properties. Therefore an accurate measurement of graphene Grüneisen parameter is of great significance for both scientific and technological interests. Compared to the previous measurements of Grüneisen parameter which showed large discrepancy [21–23], the measurement of Grüneisen parameter in our experiment was robust and could yield a value with high accuracy. This is due to the fact that unlike the uniaxial strain, the measurement of Grüneisen parameter under biaxial strain avoids the shear effect during the measurement, and is independent of Poisson ratio and not affected by the relative anisotropic shifts of Dirac cones [24, 45].

Based on equations (1) and (2), the biaxial Grüneisen parameter $\gamma$ of monolayer graphene was calculated as $\gamma_G^{SiO_2} = 2.0$, $\gamma_G^{Si_3N_4} = 1.9$, $\gamma_{2D}^{SiO_2} = 3.2$, $\gamma_{2D}^{Si_3N_4} = 3.1$, for the $G$ and $2D$ bands of graphene on

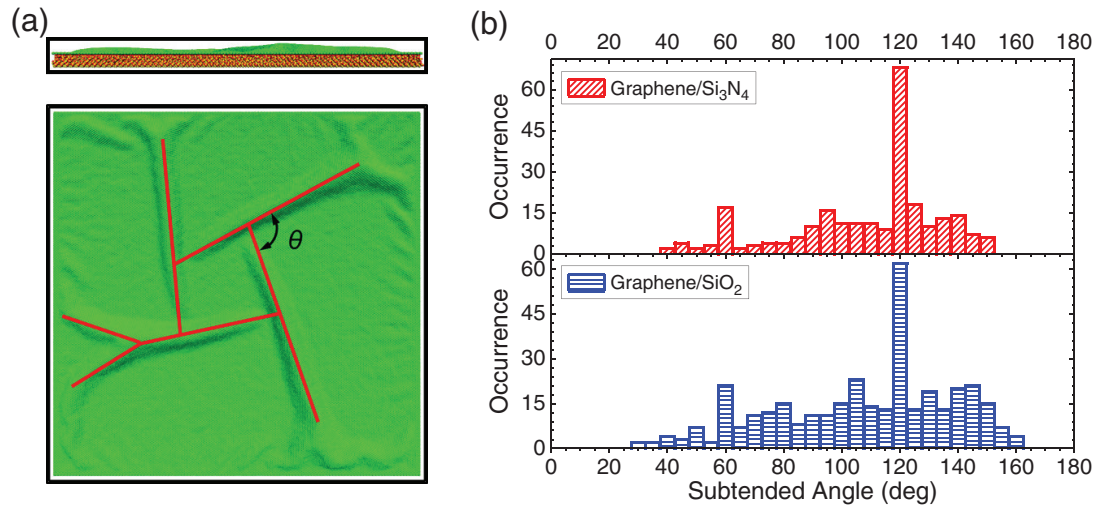


**Figure 5.** (a) Side (upper) and top (lower) views of the graphene/$SiO_2$ system considered in the MD simulations. $\theta$ designates the angle subtended by two ridges. (b) MD simulation results showing the histogram of the subtended angles between ridges for graphene/$SiO_2$ and graphene/$Si_3N_4$, respectively.

$SiO_2$ and $Si_3N_4$ substrates, respectively. It can be seen that the Grüneisen parameter values obtained using the graphene/$SiO_2$ and graphene/$Si_3N_4$ samples are very close, independent of the substrates used, as expected. Hence $\gamma_G = 1.95 \pm 0.05$ and $\gamma_{2D} = 3.15 \pm 0.05$ for the $G$ and $2D$ bands of graphene, respectively. This shows that our method for measuring biaxial Grüneisen parameter of monolayer graphene is robust. Moreover, our experimental results agree well with the theoretical values of the biaxial Grüneisen parameters of graphene calculated from first principles [45, 46].

### Biaxial compressive buckling strain of graphene

In the case of $T_H > T_S$, compressive strain is generated in graphene and the strain increases with the increase of heating temperature $T_H$ (figure 2(c)). As $T_H$ rises further, beyond a second threshold temperature $T_B$ ($>T_S$), the compressive strain in graphene might exceed the buckling strain of monolayer graphene, giving rise to the formation of buckling ridges. Figure 3 shows experimental observation of the ridges. Figures 3(a) and (b) show atomic force microscopy (AFM) images of a graphene flake on $SiO_2$ before and after the heating-cooling cycle with $T_H = 1050$ K. Figures 3(c) and (d) display AFM images of a graphene flake on $Si_3N_4$ with $T_H = 650$ K. The second threshold temperature $T_B$ was measured to be $T_B^{SiO_2} = 1040$K for graphene/$SiO_2$ and $T_B^{Si_3N_4} = 640$K for graphene/$Si_3N_4$. Substituting $T_H = T_B$ into equation (1), the compressive buckling strains of monolayer graphene were obtained as $\varepsilon_{Buckling}^{SiO_2} = 0.21\%$ and $\varepsilon_{Buckling}^{Si_3N_4} = 0.22\%$ for $SiO_2$ and $Si_3N_4$ substrates, respectively.

Also shown in figure 3 are AFM images of graphene synthesized via CVD method [52] (figure 3(e)) and epitaxial graphene on SiC synthesized via SiC sublimation [53] (figure 3(f)). It can be seen that the ridges in the synthesized graphene are virtually the same as those induced in graphene by the heating-cooling cycle. Note that during graphene synthesis via either CVD [29, 30, 52] or SiC sublimation method [31, 53], there is a cooling process from high temperature to room temperature, giving rise to compressive strain in the synthesized graphene. As the compressive strain exceeds the graphene buckling strain, buckling ridges are generated. The cooling process is similar to that in our experiments. By introducing buckling ridges in graphene using the heating-cooling cycle, our experiments can shed light on the mechanism of ridge formation in graphene synthesized by CVD [29, 30, 52] or SiC sublimation method [31, 53].

### Ridge network in graphene

The induced buckling ridges were found to form a ridge network in graphene, as shown in the high-magnification AFM images (figure 4(a)). Angle $\theta$ in figure 4(a) designates the angle subtended by two connecting ridges. Distributions of all the subtended angles were obtained for graphene/$SiO_2$ and graphene/$Si_3N_4$ respectively, as exhibited in the histograms in figure 4(b). Importantly, it was observed that for both $SiO_2$ and $Si_3N_4$ substrates the most probable subtended angle is equal to 120°, which turns out to be the highest symmetry angle of the hexagonal lattice of monolayer graphene. This implies that the crystal structure of monolayer graphene plays a key role in how the buckling ridges are formed. In other words, the compressive strain energy in graphene is relieved primarily following the symmetry directions of the graphene crystal structure. MD simulations were carried out to further understand this observation. Figure 5 shows the MD simulation results. It can be seen that the angles

subtended by the adjacent ridges are predominantly 120° (figure 5(b)), indicating that ridges formed in this configuration are most favorable in terms of the energy. The secondary most favorable peak is at 60°, which could be attributed to the symmetry of the graphene layer and the fact that 60° is the supplementary angle to 120°. The angle distribution from the MD simulations appears more continuous than that from the experiments. It might be because the simulations generate more angle data and have a much higher resolution of angles than that accessible in the experiments. The favorable angle of 120° agrees well with the reported simulation results [28].

## Conclusions

In conclusion, we systematically studied the mechanical behavior of monolayer graphene under equi-biaxial compressive strain, by thermally cycling graphene/$SiO_2$ and graphene/$Si_3N_4$ samples with a variety of heating temperatures in vacuum. At low heating temperature, graphene was perfectly bonded to substrate, leading to no strain in the graphene upon cooling to room temperature. At high heating temperature (above the first threshold temperature $T_S$), graphene slid on the substrate, which led to compressive strain in the graphene upon cooling to room temperature. The biaxial Grüneisen parameter was determined to be $\gamma_G = 1.95 \pm 0.05$ and $\gamma_{2D} = 3.15 \pm 0.05$ for $G$ and $2D$ Raman bands of graphene, respectively, regardless of the substrate. When the heating temperatures was above the second threshold temperature $T_B$, buckling ridge network was induced in graphene by the thermal cycle, with the compressive buckling strain of 0.21% and 0.22%, respectively, for graphene on $SiO_2$ and $Si_3N_4$ substrates. Both the experiments and MD simulations showed that the buckling ridges were generated in a pattern based on the lattice symmetry of monolayer graphene, with the favorable subtended angle of 120° between the buckling ridges. In addition, the thermal cycling induced graphene ridges were found reminiscent to those in graphene synthesized by CVD or SiC sublimation method, suggesting they have the same origin of formation. Our results obtained from both $SiO_2$ and $Si_3N_4$ substrates agreed very well, confirming the robustness of our method for introducing equi-biaxial compressive stress, measuring Grüneisen parameter and generating buckling ridge networks. The direct measurements of the biaxial compressive strain and induced buckling ridges for graphene on Si-based substrates could provide valuable insight into the graphene-substrate interaction, as well as design guidelines for a variety of graphene applications. This method could be extended to studying the compression behaviors of other 2D materials such as hexagonal boron nitride (BN) and transition metal dichalcogenides (e.g. $MoS_2$).

## Methods

### Experimental section

Monolayer graphene was deposited on $SiO_2$/Si (300 nm $SiO_2$) and $Si_3N_4$/Si (300 nm $Si_3N_4$) substrates by the mechanical exfoliation method [26, 32]. Monolayer graphene flakes were first identified using optical microscopy, followed by AFM characterization of thickness (Park System XE-100) [54] and Raman spectroscopy (HORIBA LabRAM HR800) [55] to confirm they are monolayer. AFM images of graphene samples were acquired using non-contact AFM mode. While measuring the strain in graphene, Raman spectroscopy was performed at the center of each graphene flake with a laser wavelength of 532 nm.

Immediately following the characterization, graphene samples were transferred into a vacuum chamber ($10^{-8}$ Torr base pressure) where it was subjected to the thermal cycling. For each cycle, the samples were heated to a heating temperature $T_H$ and then cooled down back to room temperature (295 K). The heating temperature $T_H$ was increased by an increment of 15 K between two consecutive cycles. Following each cycle, graphene sample was examined by Raman spectroscopy to measure its strain, and by AFM imaging to detect any ridge formation in it. To precisely measure the first and second threshold temperatures $T_S$ (for onset of graphene sliding) and $T_B$ (for formation of buckling ridges) respectively, when Raman shift started or buckling ridges appeared in graphene at certain heating temperature, more heating temperatures were applied with gradually decreasing temperature steps to finally determine the $T_S$ or $T_B$ within the temperature range of ±2 K.

### MD simulations

MD simulations were conducted using LAMMPS [56] to examine the buckling ridge configurations of the graphene/substrate systems under biaxial compression. The crystal structure parameters of graphene, $SiO_2$, and $Si_3N_4$ were adopted from the literature [57–59]. The interatomic interactions within graphene, $SiO_2$ and $Si_3N_4$ substrates were characterized using the Tersoff potential [60–64], while the interactions between graphene and the substrates were modeled with Lennard–Jones (LJ) potential [65]. For all simulations, the lateral ($x$-$y$ plane) domain sizes of the graphene and substrates were ~50 × 50 $nm^2$; the substrates were ~1.5 nm thick, and separated from graphene by a distance of 2Å, similar to that in previous studies of the substrate-supported graphene [66] and silicene [67]. The 2Å-thick layer of the substrate at the bottom was fixed. A strain of 1% was generated in the graphene layer by fixing its four sides. The boundary conditions in the $x$ and $y$ directions were set free, while that in the $z$ direction was set periodic. The MD time step was 0.5 fs. The equilibrium temperature and pressure of the system were 295 K and 0 bar, respectively.

In each simulation, the material system was first equilibrated as an isothermal-isobaric ensemble with the Nose–Hoover thermostat and barostat [68, 69], and then simulated as a microcanonical ensemble for data production. The average atomic positions from the last 5 ps were considered as the stable forms of the buckling ridges, and were subsequently used to examine the ridge configurations and calculate the angles subtended by the neighboring ridges. To minimize the statistical uncertainty, 40 independent simulations were carried out with different initial velocity distributions for both the graphene/$SiO_2$ and graphene/$Si_3N_4$ systems. More details about the MD simulations can be found in the supplementary material.

## Acknowledgments

This work was supported by the University of Jinan Research Initiation Fund (No. 1009405) and NSFC (No. 11628205). Y Zhu additionally acknowledges the financial support from the National Science Foundation (No. 1129817). Z Wang acknowledges the support from the National Science Foundation (No. 1150948).

## Supplementary material description

AFM and optical images of prepared monolayer graphene samples, strain mismatch between graphene and $SiO_2$, $Si_3N_4$ substrates at each heating temperature, AFM images and Raman spectra of graphene on $SiO_2$, $Si_3N_4$ substrates before and after cooling-heating cycle, AFM images and Raman spectra of graphite before and after heating-cooling cycle, and details of MD simulations of graphene buckling ridges.

## ORCID iDs

Tao Jiang https://orcid.org/0000-0002-0539-3160
Yong Zhu https://orcid.org/0000-0002-3862-5757

## References

[1] Eda G, Fanchini G and Chhowalla M 2008 Large-area ultrathin films of reduced graphene oxide as a transparent and flexible electronic material *Nat. Nanotechnol.* **3** 270
[2] Kim K S, Zhao Y, Jang H, Lee S Y, Kim J M, Kim K S, Ahn J H, Kim P, Choi J Y and Hong B H 2009 Large-scale pattern growth of graphene films for stretchable transparent electrodes *Nature* **457** 706
[3] Sun Z, Zhang J, Yin L, Hu G, Fang R, Cheng H M and Li F 2017 Conductive porous vanadium nitride/graphene composite as chemical anchor of polysulfides for lithium-sulfur batteries *Nat. Commun.* **8** 14627
[4] Torres T 2017 Graphene chemistry *Chem. Soc. Rev.* **46** 4385–6
[5] Sun H *et al* 2017 Three-dimensional holey-graphene/niobia composite architectures for ultrahigh-rate energy storage *Science* **356** 599–604
[6] Han S, Wu D, Li S, Zhang F and Feng X 2014 Porous graphene materials for advanced electrochemical energy storage and conversion devices *Adv. Mater.* **26** 849–64
[7] Teague M L *et al* 2009 Evidence for strain-induced local conductance modulations in single-layer graphene on $SiO_2$ *Nano Lett.* **9** 2542–6
[8] Min K and Aluru N R 2011 Mechanical properties of graphene under shear deformation *Appl. Phys. Lett.* **98** 013113
[9] Klimov N N *et al* 2012 Electromechanical properties of graphene drumheads *Science* **336** 1557–61
[10] Akinwande D *et al* 2017 A review on mechanics and mechanical properties of 2D materials—graphene and beyond *Extreme Mech. Lett.* **13** 42–77
[11] Ni Z H, Yu T, Lu Y H, Wang Y Y, Feng Y P and Shen Z X 2008 Uniaxial strain on graphene: Raman spectroscopy study and band-gap opening *ACS Nano* **2** 2301–5
[12] Zhou S Y, Gweon G H, Fedorov A V, First P D, De Heer W A, Lee D H, Guinea F, Neto A C and Lanzara A 2007 Substrate-induced bandgap opening in epitaxial graphene *Nat. Mater.* **6** 770
[13] Guinea F, Katsnelson M I and Geim A K 2010 Energy gaps and a zero-field quantum Hall effect in graphene by strain engineering *Nat. Phys.* **6** 30
[14] Guassi M R, Diniz G S, Sandler N and Qu F 2015 Zero-field and time-reserval-symmetry-broken topological phase transitions in graphene *Phys. Rev.* B **92** 075426
[15] Amorim B *et al* 2016 Novel effects of strains in graphene and other two dimensional materials *Phys. Rep.* **617** 1–54
[16] Gomes K K, Mar W, Ko W, Guinea F and Manoharan H C 2012 Designer Dirac fermions and topological phases in molecular graphene *Nature* **483** 306
[17] Levy N, Burke S A, Meaker K L, Panlasigui M, Zettl A, Guinea F, Neto A C and Crommie M F 2010 Strain-induced pseudo-magnetic fields greater than 300 tesla in graphene nanobubbles *Science* **329** 544–7
[18] Zhu S, Stroscio J A and Li T 2015 Programmable extreme pseudomagnetic fields in graphene by a uniaxial stretch *Phys. Rev. Lett.* **115** 245501
[19] Si C, Liu Z, Duan W and Liu F 2013 First-principles calculations on the effect of doping and biaxial tensile strain on electron–phonon coupling in graphene *Phys. Rev. Lett.* **111** 196802
[20] Kauppila V J, Aikebaier F and Heikkilä T T 2016 Flat-band superconductivity in strained Dirac materials *Phys. Rev.* B **93** 214505
[21] Metzger C *et al* 2010 Biaxial strain in graphene adhered to shallow depressions *Nano Lett.* **10** 6–10
[22] Zabel J *et al* 2012 Raman spectroscopy of graphene and bilayer under biaxial strain: bubbles and balloons *Nano Lett.* **12** 617–21
[23] Ferralis N 2010 Probing mechanical properties of graphene with Raman spectroscopy *J. Mater. Sci.* **45** 5135–49
[24] Frank O *et al* 2010 Compression behavior of single-layer graphenes *ACS Nano* **4** 3131–8
[25] Androulidakis C *et al* 2014 Failure processes in embedded monolayer graphene under axial compression *Sci. Rep.* **4** 5271
[26] Jiang T, Huang R and Zhu Y 2014 Interfacial sliding and buckling of monolayer graphene on a stretchable substrate *Adv. Funct. Mater.* **24** 396–402
[27] Guo G and Zhu Y 2015 Cohesive-shear-lag modeling of interfacial stress transfer between a monolayer graphene and a polymer substrate *J. Appl. Mech.* **82** 031005
[28] Zhang K and Arroyo M 2014 Understanding and strain-engineering wrinkle networks in supported graphene through simulations *J. Mech. Phys. Solids* **72** 61–74
[29] Huang P Y *et al* 2011 Grains and grain boundaries in single-layer graphene atomic patchwork quilts *Nature* **469** 389
[30] Li X *et al* 2009 Large-area synthesis of high-quality and uniform graphene films on copper foils *Science* **324** 1312–4
[31] Oida S, Hannon J B and Tromp R M 2014 Controlled synthesis and decoupling of monolayer graphene on SiC(0 0 0 1) *Appl. Phys. Lett.* **104** 161605
[32] Novoselov K S *et al* 2005 Two-dimensional atomic crystals *Proc. Natl Acad. Sci.* **102** 10451–3
[33] Jiang T and Zhu Y 2015 Measuring graphene adhesion using atomic force microscopy with a microsphere tip *Nanoscale* **7** 10760–6

[34] Zong Z, Chen C L, Dokmeci M R and Wan K T 2010 Direct measurement of graphene adhesion on silicon surface by intercalation of nanoparticles *J. Appl. Phys.* **107** 026104
[35] Koenig S P, Boddeti N G, Dunn M L and Bunch J S 2011 Ultrastrong adhesion of graphene membranes *Nat. Nanotechnol.* **6** 543
[36] Yoon D, Son Y W and Cheong H 2011 Negative thermal expansion coefficient of graphene measured by Raman spectroscopy *Nano Lett.* **11** 3227–31
[37] Budrikis Z and Zapperi S 2016 Temperature-dependent adhesion of graphene suspended on a trench *Nano Lett.* **16** 387–91
[38] López-Polín G, Ortega M, Vilhena J G, Alda I, Gomez-Herrero J, Serena P A, Gomez-Navarro C and Pérez R 2017 Tailoring the thermal expansion of graphene via controlled defect creation *Carbon* **116** 670–7
[39] Gong L, Kinloch I A, Young R J, Riaz I, Jalil R and Novoselov K S 2010 Interfacial stress transfer in a graphene monolayer nanocomposite *Adv. Mater.* **22** 2694–7
[40] Conley H, Lavrik N V, Prasai D and Bolotin K I 2011 Graphene bimetallic-like cantilevers: probing graphene/substrate interactions *Nano Lett.* **11** 4748–52
[41] Tsoukleri G *et al* 2009 Subjecting a graphene monolayer to tension and compression *Small* **5** 2397–402
[42] Ferrari A C and Basko D M 2013 Raman spectroscopy as a versatile tool for studying the properties of graphene *Nat. Nanotechnol.* **8** 235–46
[43] Neumann C *et al* 2014 Raman spectroscopy as probe of nanometre-scale strain variations in graphene *Nat. Commun.* **6** 8429
[44] Huang M, Yan H, Chen C, Song D, Heinz T F and Hone J 2009 Phonon softening and crystallographic orientation of strained graphene studied by Raman spectroscopy *PNAS* **106** 7304–8
[45] Mohiuddin T M G *et al* 2009 Uniaxial strain in graphene by Raman spectroscopy: G peak splitting Grüneisen parameters and sample orientation *Phys. Rev.* B **79** 205433
[46] Mounet N and Marzari N 2005 First-principles determination of the structural, vibrational and thermodynamic properties of diamond, graphite, and derivatives *Phys. Rev.* B **71** 205214
[47] Standard Reference Material 739, Fused-silica thermal expansion, National Institute of Standards and Technology, U.S. Department of Commerce, Gaithersburg, MD (27 December 1991) (www-s.nist.gov/srmors/certificates/archives/739.pdf)
[48] Paszkowicz W *et al* 2004 Thermal expansion of spinel-type $Si_3N_4$ *Phys. Rev.* B **69** 052103
[49] Shaina P R, George L, Yadav V and Jaiswal M 2016 Estimating the thermal expansion coefficient of graphene: the role of graphene-substrate interactions *J. Phys.: Condens. Matter* **28** 085301
[50] Jean F, Zhou T, Blanc N, Felici R, Coraux J and Renaud G 2013 Effect of preparation on the commensurabilities and thermal expansion of graphene on Ir (1 1 1) between 10 and 1300 K *Phys. Rev.* B **88** 165406
[51] Pozzo M, Alfe D, Lacovig P, Hofmann P, Lizzit S and Baraldi A 2011 Thermal expansion of supported and freestanding graphene: lattice constant versus interatomic distance *Phys. Rev. Lett.* **106** 135501
[52] Obraztsov A N, Obraztsova E A, Tyurnina A V and Zolotukhin A A 2007 Chemical vapor deposition of thin graphite films of nanometer thickness *Carbon* **45** 2017–21
[53] Prakash G, Capano M A, Bolen M L, Zemlyanov D and Reifenberger R G 2010 AFM study of ridges in few-layer epitaxial graphene grown on the carbon-face of 4H–SiC *Carbon* **48** 2383–93
[54] Obraztsova E A, Osadchy A V, Obraztsova E D, Lefrant S and Yaminsky I V 2008 Statistical analysis of atomic force microscopy and Raman spectroscopy data for estimation of graphene layer numbers *Phys. Status Solidi* B **245** 2055–9
[55] Graf D *et al* 2007 Spatially resolved Raman spectroscopy of single- and few- layer graphene *Nano Lett.* **7** 238–42
[56] Plimpton S 1995 Fast parallel algorithms for short-range molecular dynamics *J. Comput. Phys.* **117** 1–19
[57] Tersoff J 1988 New empirical approach for the structure and energy of covalent systems *Phys. Rev.* B **37** 6991–7000
[58] Munetoha S, Motookaa T, Moriguchib K and Shintanic A 2007 Interatomic potential for Si–O systems using Tersoff parameterization *Comput. Mater. Sci.* **39** 334–9
[59] de Brito Mota F, Justo J F and Fazzio A 1998 Structural properties of amorphous silicon nitride *Phys. Rev.* B **58** 8323–8
[60] Kinaci A, Haskins J B, Sevik C and Cagin T 2012 Thermal conductivity of BN–C nanostructures *Phys. Rev.* B **86** 115410
[61] Lindsay L and Broido D A 2010 Optimized Tersoff and Brenner empirical potential parameters for lattice dynamics and phonon thermal transport in carbon nanotubes and graphene *Phys. Rev.* B **81** 205441
[62] Rappe A K, Casewit C J, Colwell K S, Goddard W A III and Skiff W M 1992 UFF, a full periodic table force field for molecular mechanics and molecular dynamics simulations *J. Am. Chem. Soc.* **114** 10024–35
[63] Cooper D R *et al* 2012 Experimental review of graphene *ISRN Condens. Matter Phys.* **2012** 1–56
[64] Hatch D M and Ghose S 1991 The $\alpha$-$\beta$ phase transition in cristobalite, $SiO_2$ *Phys. Chem. Miner.* **17** 554–62
[65] Grun R 1979 The crystal structure of $\beta$-$Si_3N_4$: structural and stability considerations between $\alpha$- and $\beta$-$Si_3N_4$ *Acta Cryst.* **35** 800–4
[66] Qiu B and Ruan X 2012 Reduction of spectral phonon relaxation times from suspended to supported graphene *Appl. Phys. Lett.* **100** 193101
[67] Wang Z, Feng T and Ruan X 2015 Thermal conductivity and spectral phonon properties of freestanding and supported silicene *J. Appl. Phys.* **117** 084317
[68] Nose S 1984 A unified formulation of the constant temperature molecular dynamics methods *J. Chem. Phys.* **81** 511–9
[69] Hoover W G 1985 Canonical dynamics: equilibrium phase-space distributions *Phys. Rev.* A **31** 1695–7